eurasia

**SUPPLEMENTARY DATA**

Check for updates

# A nano-enclatherated-gel-composite for the treatment of alcohol abuse and addiction

**Fatema Mia, Mershen Govender, Sunaina Indermun, Pradeep Kumar, Lisa C. du Toit, Yahya E. Choonara***

*Wits Advanced Drug Delivery Platform Research Unit, Department of Pharmacy and Pharmacology, School of Therapeutic Sciences, Faculty of Health Sciences, University of the Witwatersrand, Johannesburg, 7 York Road, Parktown 2193, South Africa*
*\*Corresponding Author: Professor Yahya E. Choonara; Tel: +27-11-717-2052; Fax: +27-11-642-4355. Email: Yahya.Choonara@wits.ac.za*

## S.1. Methods

### S.1.1. Disulfiram-loaded TPGS nanomicelles

#### S.1.1.1. Experimental Design

A two factor, three level Face Centred Central Composite Design (FCCCD) was generated by Minitab® statistical software (V15, Minitab Inc., PA, USA) for statistical optimization of the Disulfiram-loaded TPGS nanomicelles. The input factors generated 13 experimental runs (Table S1). In the design the stirring time (1-5 hours) and the

| Formulation Number | TPGS amount (mg) | Stirring Time (hours) |
|---|---|---|
| 1 | 750 | 3 |
| 2 | 500 | 1 |
| 3 | 500 | 5 |
| 4 | 750 | 1 |
| 5 | 1000 | 3 |
| 6 | 750 | 3 |
| 7 | 500 | 3 |
| 8 | 1000 | 1 |
| 9 | 750 | 3 |
| 10 | 750 | 3 |
| 11 | 1000 | 5 |
| 12 | 750 | 3 |
| 13 | 750 | 5 |

**Table S1.** Formulations generated using a Face Centred Central Composite statistical design for the optimization of disulfiram-loaded nanomicelles.

amount of polymer used (500-1000mg) were taken as the independent variables whilst drug loading (%), entrapment efficiency (%) and drug release (%) were taken as the dependent parameters. The FCCCD optimization output indicated utilization of 500mg TPGS with a stirring time of 1 hour in order to generate optimized nanomicelles.

#### S.1.1.2. Drug entrapment efficiency and drug loading capacity

A ratio of Simulated Body Fluid (SBF; pH 7.4) to acetone was utilized as both a disulfiram extraction medium and a disulfiram-absorbance detector for all UV analyses and was prepared to adequately simulate intramuscular conditions according to the method by Marques and co-workers [1]. The acetone-buffer solution (ABS) was made of acetone to SBF buffer in a ratio of 1:18. Disulfiram-loaded nanomicelles were added to 10mL of SBF and stirred for 48 hours at 37°C using a magnetic stirrer. Chloroform (10mL) was thereafter added to the mixture and the formulation was vigorously shaken to completely extract the disulfiram. The emulsion was allowed to separate, the chloroform layer was syringed out, and left to dry to allow for evaporation of the chloroform. The remaining solid, containing the drug, was reconstituted with 40mL of the extraction medium (i.e. ABS) with the absorbance tested at 262nm ($\varepsilon = 110.0857$) using UV spectroscopy (Implen NanophotometerTM, Implen GmbH, München, Germany). The entrapment efficiency (EE%) and drug loading (DL%) of the formulations was subsequently determined.

### S.1.1.3. Differential Scanning Calorimetry

The DSC curves were generated with a Differential Scanning Calorimeter (Mettler Toledo) fitted with Stare software (Mettler Toledo, Switzerland). The thermal transitions of native TPGS and disulfiram were compared to the TPGS-disulfiram nanomicelle mixture. Accurately weighed samples (±10mg) were placed into standard 40μL aluminum crucibles. The crucibles were perforated and hermetically sealed. Samples were then heated at a heating rate of 10°C/minute between a temperature range of 0-300°C under a constant purge of inert nitrogen.

### S.1.1.4. X-Ray Diffraction analysis

The crystalline or amorphous disposition of the individual components as well as nanomicelles were determined using X-Ray diffraction patterns. The diffractograms were obtained using a Benchtop X-Ray Diffractometer (Rigaku Miniflex 600, Rigaku Corporation, Matsubara-cho, Akishima-shi, Tokyo, Japan). The measurement parameters were a 10mm Incident Height Slit (IHS), 1.25° Divergence Slit (DS), 13mm Solar Slit (SS) and 13mm Receiving Slit (RS). The diffractometer was operated using the Rigaku MiniFlex Guidance software, version 1.2.0.0. All experimental procedures were conducted over a diffraction angle range of 0º-90º 2θ. Integrated X-ray powder diffraction software (PDXL 2.1, Rigaku Corporation, Matsubara-cho, Akishima-shi, Tokyo, Japan) was used for data acquisition and analysis. The experimental temperature was maintained at 19ºC.

### S.1.2. UPLC conditions analysis

UPLC analysis of the blood was accomplished by using a Waters Acquity® UPLC system (Waters, Milford, MA, USA) coupled with a photoiodide array detector (PDA) and Empower® Pro Software (Waters, Milford, MA, USA). The UPLC was fitted with an Acquity® UPLC BEH C18 column, with a particle size of 1.7μm and a pore size of 130Å. The chromatographic conditions implemented were derived from methods outlined by Zhang and co-workers [2] and Spivak and co-workers [3]. The mobile phase consisted of 0.1% formic acid in double deionised water and 0.1% formic acid in methanol (50:50). Drug detection was carried out at a temperature

of 40°C. An isocratic method was employed for the separation, identification and quantification of drug with a flow rate of 0.5mL/min, an injection volume of 10μL and a run time of 6 minutes. The PDA detector was set at a wavelength of 262nm for the detection of disulfiram. Diclofenac was selected as the internal standard (IS).

## S.2. Results and Discussion

### S.2.1. Disulfiram-loaded TPGS nanomicelles

### S.2.1.1. Drug loading and drug entrapment

The drug loading percentage of the formulations ranged from 14.41-33.41 (SD ≤ 23.22, n = 3 in all cases). The percentage drug loading for each formulation of the FCCD is displayed in Fig. S.1.

At medium-low TPGS amounts the drug loading percentage and entrapment efficiency percentage decreased with an increased stirring time. The entrapment percentage of disulfiram into nanomicelles ranged from 24.92-58.46% (SD ≤ 14.12, n = 3 in all cases). The entrapment efficiency for each formulation is displayed in Fig. S.2.

### S.2.1.2. In vitro drug release profiles

The percentage cumulative release over 28 days for the 13 design formulations is displayed in Fig. S.3 (SD ≤ 22.88 in all cases, n = 3). The fastest release was from DF1 followed by DF9 and DF3. The slowest release was seen in DF7. An initial burst release on the first day was seen in all formulations. This may be due to the poorly entrapped drug that is adsorbed to the surface of
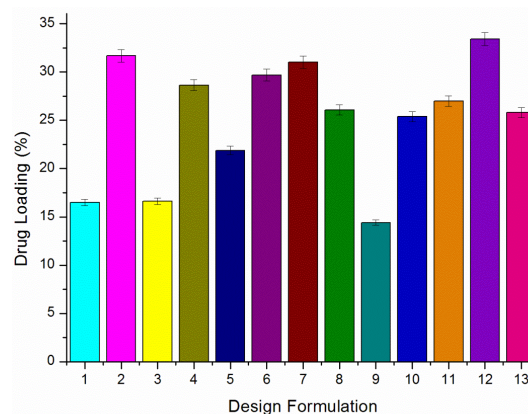


**Figure S.1.** Drug loading % for each formulation of the FCCD.

the micelles [4]. A general trend that was present was that at low drug loading and entrapment efficiency percentages, the faster the release and the higher the entrapment efficiency and drug loading the slower the release. This can be attributed to the fact that in those formulations with higher entrapment efficiency and drug loading a greater amount of drug was well encapsulated in the micelle core thus requiring a longer time to be released from the micelle and into the dissolution medium. Those with less drug need less time to release the drug that is contained in the micelle thus the faster release rate.
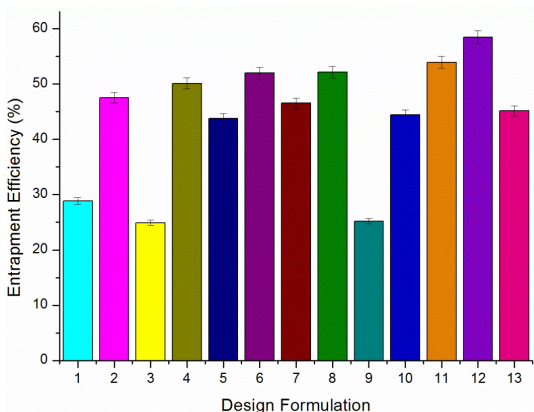


**Figure S.2.** Entrapment efficiency % for each formulation of the FCCD.

### S.2.1.3. Particle size

Particle size analysis was conducted on the 13 design formulations in order to confirm that the micelles fabricated fell into the correct size range for nanomicelle viz. 10-100nm [5]. The micelle sizes and Poly Dispersity Index (PDI) are recorded in Table S.2. Examination of the results showed that sizes ranged from

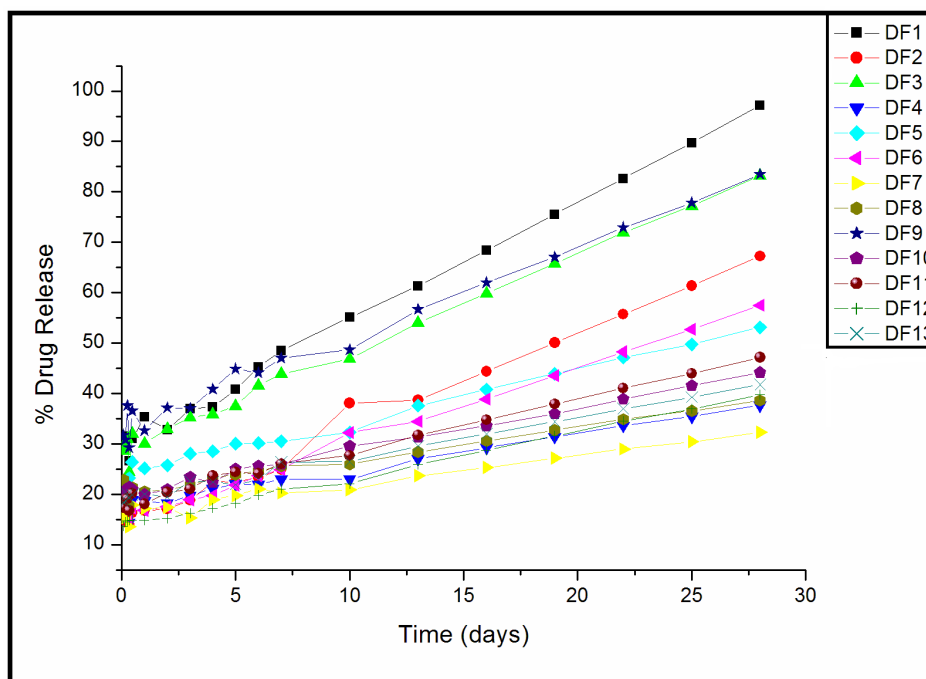| Design Formulation Number | Particle Size (nm) | PDI |
|---|---|---|
| 1 | 23.36 | 0.26 |
| 2 | 25.09 | 0.25 |
| 3 | 31.2 | 0.42 |
| 4 | 18.09 | 0.21 |
| 5 | 19.96 | 0.35 |
| 6 | 17.05 | 0.26 |
| 7 | 22.95 | 0.35 |
| 8 | 24.14 | 0.36 |
| 9 | 15.26 | 0.25 |
| 10 | 17.55 | 0.26 |
| 11 | 17.25 | 0.22 |
| 12 | 15.56 | 0.19 |
| 13 | 16.44 | 0.24 |

**Table S.2.** Particle sizes and PDI values.



**Figure S.3.** Cumulative disulfiram release from DF1-DF13 over 28 days.

130

15.26nm - 31.20nm (SD ≤ 3.77, n=3). Thus all formulations are within the acceptable range for polymeric nanomicelles. There was no noticeable trend in particle size change due to change in polymer amount or stirring time. This was also observed by Muthu et al. [6]. The PDI's ranged from 0.19-0.42 (SD ≤ 0.094, n=3) which indicates narrow size distribution. Sizes obtained were in accordance with those previously reported [7,8]

### S.2.1.4. Thermal profile analysis of the nanomicelles

The native TPGS thermogram displays two phenomena (Fig. S.4). The first is an endothermic peak at 38°C, representative of the melting point (Tm) of TPGS. This Tm value indicates the crystalline nature of TPGS [9]. The second thermal event has an onset at 215.6°C, denoting the thermal non-oxidative degradation temperature of TPGS. These findings are in agreement with reported thermal behavior for TPGS [10]. The high degradation temperature of TPGS implies that it is a fitting choice of polymer as it is thermally stable under standard processing temperatures utilized in pharmaceutical application [11]. The blank nanomicelle thermogram shares
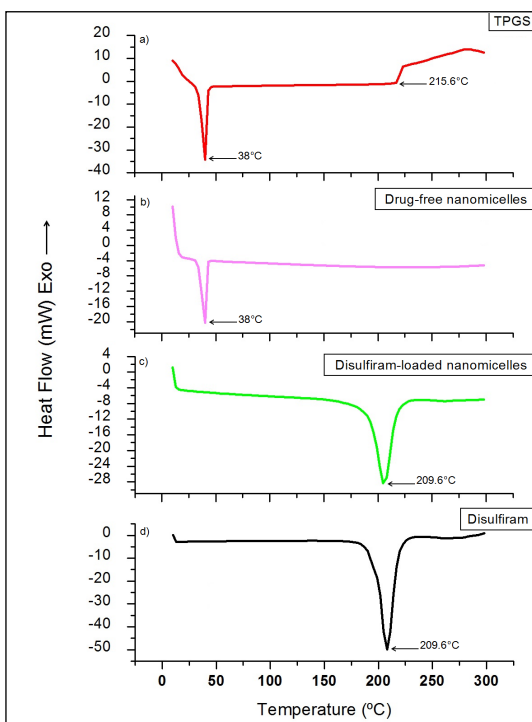
similarity to the native TPGS curve. The one major difference is the absence of the degradation peak. The Tm peak of the blank nanomicelles is present at the same temperature (38°C) as that of pure TPGS. There is no change in the peaks nor are there any new peaks. This emergence of the TPGS peak without any change in the peak or new peaks indicates that the TPGS structure is maintained and is present intact in the drug-free nanomicelles [12]. The disulfiram thermogram displays an endothermic peak at 209.6°C, indicating the decomposition of disulfiram. The disulfiram-loaded nanomicelles also display the same event indicating that disulfiram is present in the nanomicelle.

### S.2.1.5. XRD analysis

The XRD diffractogram of TPGS displays two sharp peaks at 19° and 23° (Fig. S.5), indicative of the crystal nature of TPGS [13]. These peaks correspond to the semi-crystalline polyethylene glycol chains of TPGS. Drug-free nanomicelles displayed the defining peaks of pure TPGS. The decrease in intensity is representative of a slight decrease in crystallinity. The overall profile is not significantly different to that of native TPGS. The disulfiram diffractogram displays a large number of sharp, high
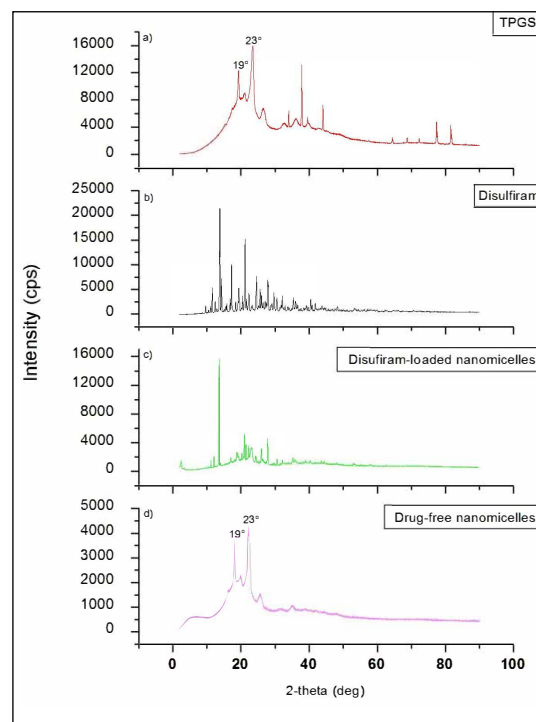


**Figure S.4.** Thermograms of **a)** TPGS, **b)** drug-free nanomicelles, **c)** disulfiram-loaded nanomicelles and **d)** pure disulfiram.



**Figure S.5.** Diffractograms of **a)** TPGS, **b)** disulfiram, **c)** disulfiram-loaded nanomicelles and **d)** drug free nanomicelles.

intensity diffraction peaks symbolizing the highly crystalline nature of disulfiram. The diffractogram for disulfiram-loaded nanomicelles displays the peaks of both disulfiram and TPGS. Both components have retained their crystallinity with the very sharp peaks being attributed to disulfiram and those that are slightly broader being attributed to TPGS. It is evident from the diffractograms that nanomicelles prepared using the solvent casting method has had no effect on the physical state of the active as well as the polymer. Whilst both still maintain a predominantly crystal state the decrease in intensity is synonymous with a decrease in crystallinity. This could be due to the method of preparation by which both components were dissolved in chloroform and in doing so both were maintained in the dissolved state upon chloroform extraction [14].

### S.2.2. Macroscopic examination of the gel

At low temperatures (A) the formulation is more liquid-like and at room temperature (B) the formulation is less liquid-like (Fig. S.6). At body temperature (C) the formulation has solidified into a gel (no movement upon tilting of the vial). The gel is opaque as is expected due to the inclusion of HAGG. Gels are homogenous in appearance without the presence of any lumps or air bubbles which is an important aspect to consider in parenteral delivery systems.

### S.2.3. NEGC System

#### S.2.3.1. Fourier Transform Infrared spectroscopy analysis of the NEGC

FTIR was conducted to ascertain that the structural properties of the optimized system were preserved during the formulation of the NEGC. In the HAGG gel, the band at $3295cm^{-1}$ (peak 1) signifies H-bonded O-H stretch vibrations of hydroxyl groups. At $2888cm^{-1}$ (peak 2) for LA and $2930cm^{-1}$ (peak 6) for HA there are C-H stretching bands of CH and $CH_2$ present. Bands of $1600cm^{-1}$ (peak 3) HAGG can be attributed to asymmetric carboxylate anion stretching. The $1019cm^{-1}$ band (peak 10) in HAGG denote C-O stretching vibrations. A prominent HAGG additional peak that is not present in LAGG is $1724cm^{-1}$ (peak 7), which can be attributed to a carbonyl group indicating C=O. HAGG displays a band at $1380cm^{-1}$ (peak 8) which signifies methyl C-H bonding and $1280cm^{-1}$ (peak 9) which signifies C-O-C vibrations (Fig. S.7).



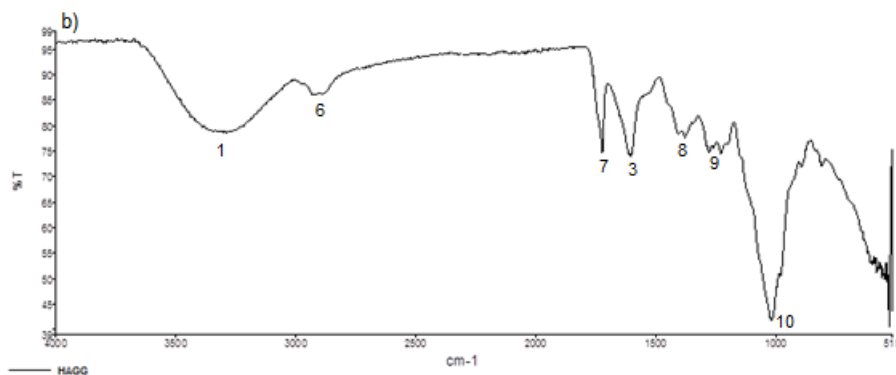**Figure S.6.** PF127-HAGG formulation at 10°C **(A)**, 25°C **(B)** and 37.5°C **(C)**.



**Figure S.7.** FTIR spectra of HAGG.

Fig. S.8 displays the FTIR spectra of all the components as well as the various combinations. PF127 displays a band at 2878cm$^{-1}$ (peak 1) which can be attributed to C-H stretching vibrations. 1466cm$^{-1}$ (peak 2) signifies $CH_2$ and $CH_3$ bending. O-H in plane bending is represented by 1341cm$^{-1}$ (peak 3). The peak at 1095cm$^{-1}$ (peak 4) can be ascribed to R-O stretching. Minimal changes are present confirming that structural integrity was not compromised during the formation of the NEGC and the other composites. The spectra at 10°C were not included as they were identical to those at 36.5°C.

### S.2.3.2. Thermal profile analysis

A thermal description of HAGG, PF127-GG gel and combinations of the gel with pure disulfiram and nanomicelles (drug-free nanomicelles and disulfiram-loaded nanomicelles) was obtained through DSC. Both forms of GG display an endothermic peak and a pronounced exothermic peak. The endothermic peak is present at 106.3°C HAGG and the exothermic peak is at 250°C. The endothermic event signifies a dehydration process whereby loss of absorbed moisture occurs [15]. The exothermic occurrence represents degradation whereby decomposition without melting occurs. This is confirmed by the amorphous structure of GG and amorphous materials lack a distinct melting point. This thermal degradation occurs as a result of disintegration of molecular chains. HAGG has an additional endothermic peak at 182.2°C (Fig. S.9a). PF127 has a characteristic endothermic peak at 56.3°C [16]. This peak is the $T_m$ of PF127 proving that PF127 has a crystalline structure (Fig. S.9b).

Similarities in the DSC thermograms indicate the absence of chemical. Combination formulations maintained chemical integrity as is evident by the similar DSC profile of each compared to the native constituents. Furthermore, change from the liquid state to solid state did not a have a profound effect as thermograms for both temperatures (i.e. 10°C and 36.5°C are identical (Fig. S.10).

### S.2.3.3. XRD Analysis

The HAGG diffractogram displays crystalline peaks at 9° and 20° (Fig. S.11a). The intensity of the HAGG peaks are low, side-by-side association and crystallization is sterically inhibited by acylation. This reduces the extent of the gel's crystallinity leading to decreased brittleness and increased elasticity. Packing of the helices is prevented by the bulky L-glycerate ester
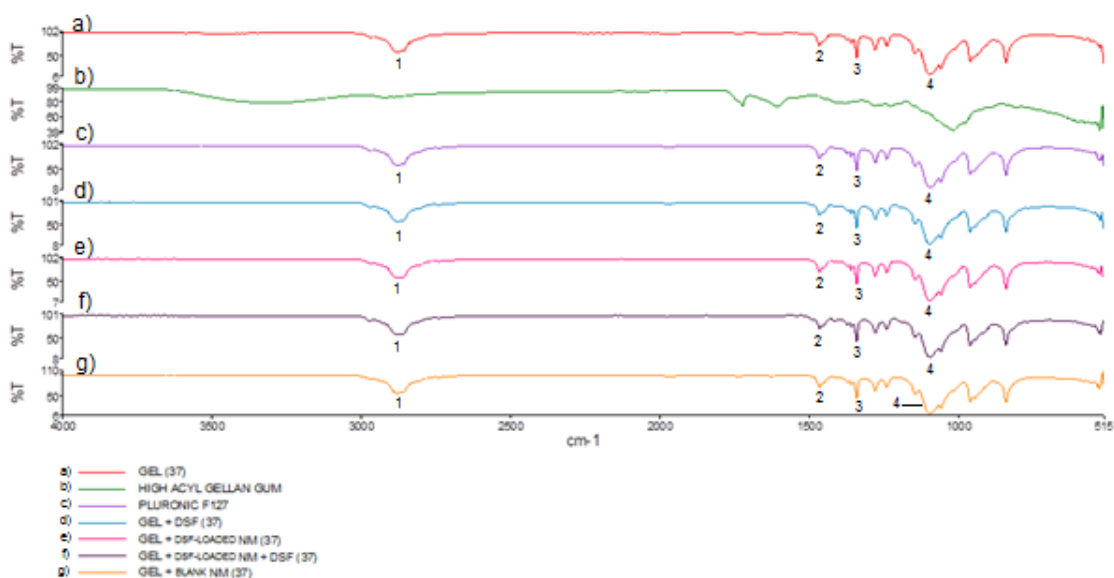


**Figure S.8.** FTIR spectra of the native components of the NEGC as well as the combined NEGC and its variations.
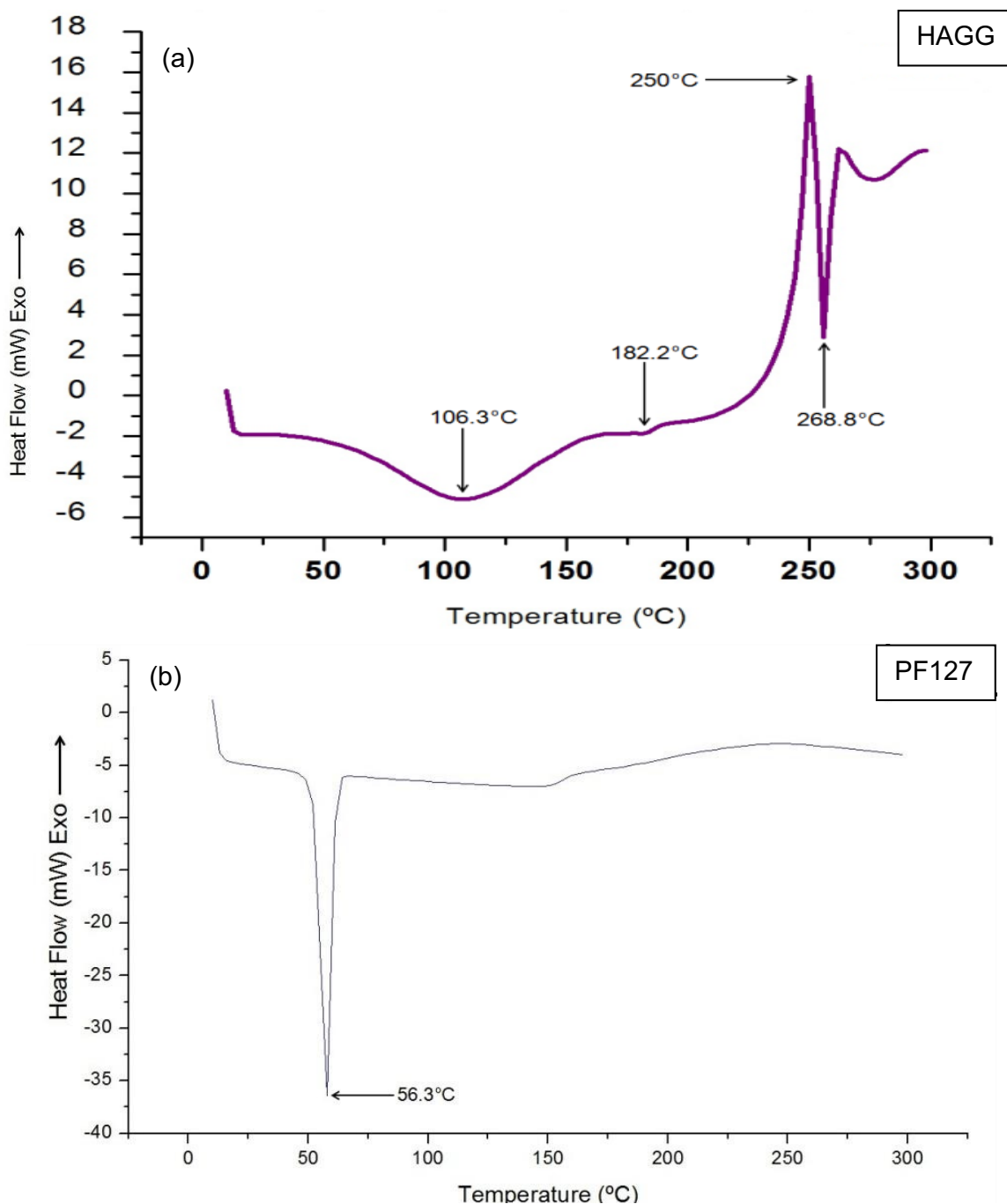
**Figure S.9.**　Thermograms of **a)** HAGG and **b)** PF127.

groups in the unit cell. PF127 also possesses two distinct diffraction peaks at 19° and 23° (Fig. S.11b). These are due to the presence of PEO groups in the polymer [16]. These peaks illustrate the crystal structure of PF127. As can be seen from the various combined formulations at different temperatures similarities exist across all (Fig. S.11c). Peaks that are identically positioned in the mixture indicate that there was no interference of the drug with lattice spacing of the polymer.
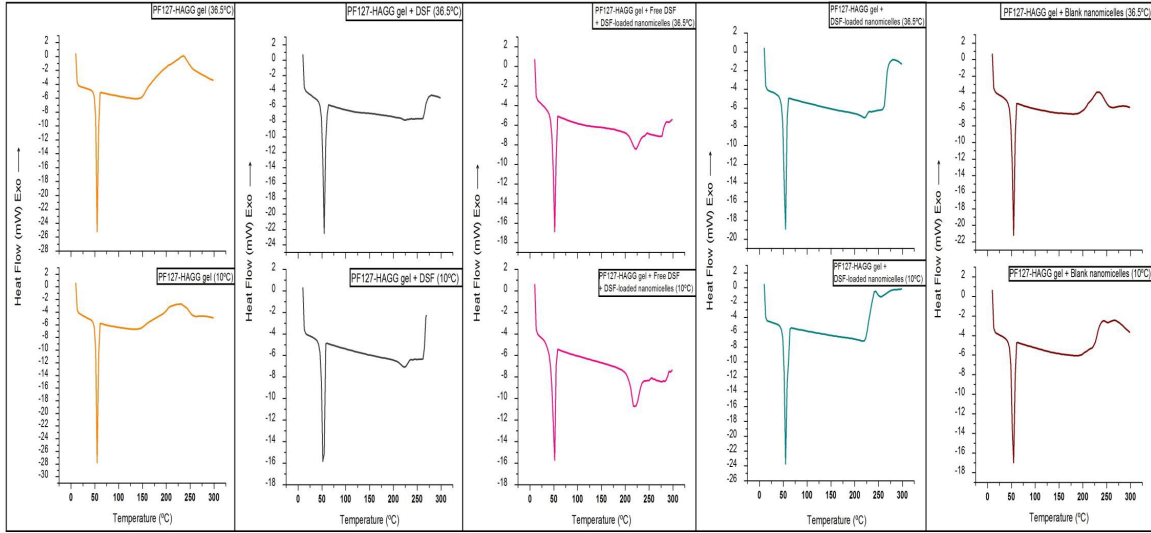
**Figure S.10.** Thermograms of various combinations of gel, nanomicelles and disulfiram at 36.5°C (top row) and 10°C (bottom row).
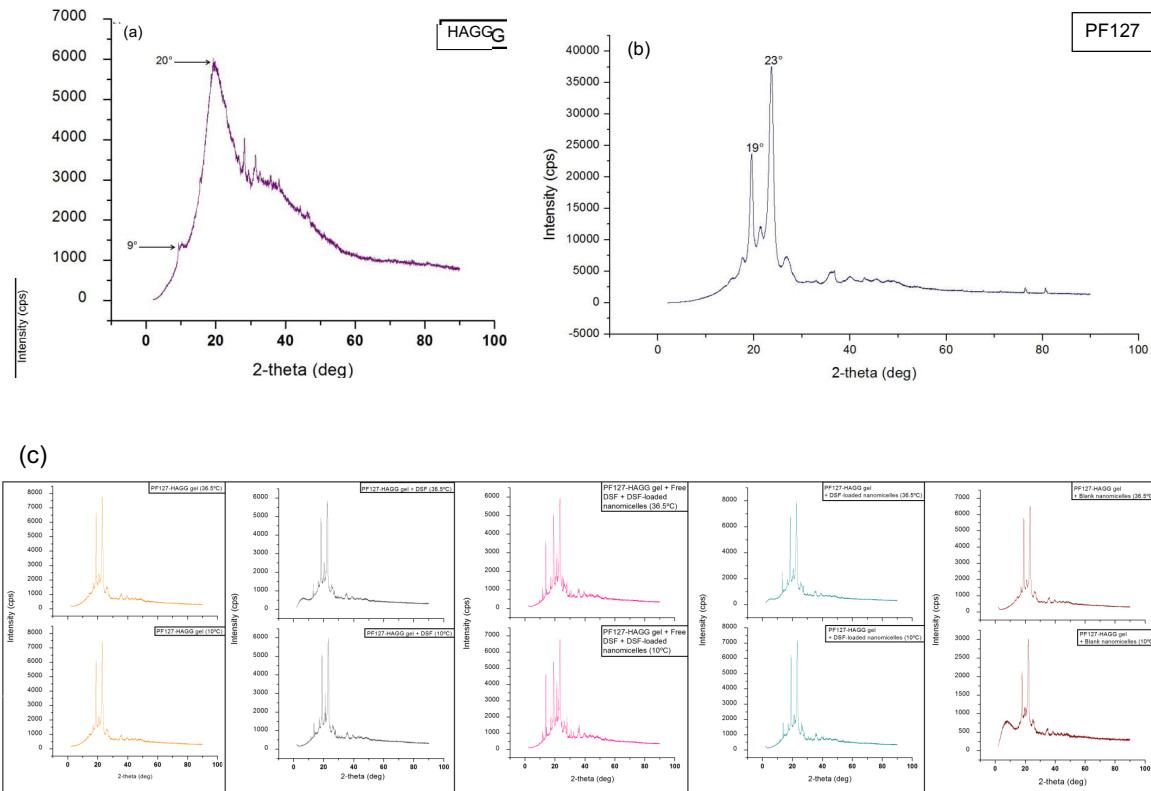


**Figure S.11.** Diffractograms of **(a)** HAGG **(b)** PF127 **(c)** various combinations of gel, nanomicelles and disulfiram at 36.5°C (top row) and 10°C (bottom row).

## References

1. Marques MR, Loebenberg R, Almukainzi M. Simulated biological fluids with possible application in dissolution testing. Dissolution Technol. 2011;18(3):15-28. doi:10.14227/DT180311P15.

2. Zhang L, Jiang Y, Jing G, Tang Y, Chen X, Yang D, Zhang Y, Tang X. A novel UPLC–ESI-MS/MS method for the quantitation of disulfiram, its role in stabilized plasma and its application. J. Chromatogr. B Biomed. Appl. 2013;937:54-9. doi:10.1016/j.jchromb.2013.08.009.

3. Spivak AM, Andrade A, Eisele E, Hoh R, Bacchetti P, Bumpus NN, Emad F, Buckheit R, McCance-Katz EF, Lai J, Kennedy M, Chander G, Siliciano RF, Siliciano JD, Deeks SG. A pilot study assessing the safety and latency-reversing activity of disulfiram in HIV-1–infected adults on antiretroviral therapy. Clin. Infect. Dis. 2014;58(6):883-90. doi:10.1093/cid/cit813.

4. Zeng X, Tao W, Mei L, Huang L, Tan C, Feng S-S. Cholic acid-functionalized nanoparticles of star-shaped PLGA-vitamin E TPGS copolymer for docetaxel delivery to cervical cancer. Biomaterials 2013;34(25):6058-67. doi:10.1016/j.biomaterials.2013.04.052.

5. Mohamed S, Parayath NN, Taurin S, Greish K. Polymeric nano-micelles: versatile platform for targeted delivery in cancer. Ther. Deliv. 2014;5(10):1101-21. doi:10.4155/tde.14.69.

6. Muthu MS, Avinash Kulkarni S, Liu Y, Feng S.S. Development of docetaxel-loaded vitamin E TPGS micelles: formulation optimization, effects on brain cancer cells and biodistribution in rats. Nanomedicine (Lond) 2012;7(3):353-64. doi:10.2217/nnm.11.111.

7. Butt AM, Amin MCIM, Katas H, Sarisuta N, Witoonsaridsilp W, Benjakul R. In vitro characterization of pluronic F127 and D-α-tocopheryl polyethylene glycol 1000 succinate mixed micelles as nanocarriers for targeted anticancer-drug delivery. J. Nanomater. 2012;916573. doi:10.1155/2012/916573.

8. Sonali, Agrawal P, Singh RP, Rajesh CV, Singh S, Vijayakumar MR, Pandey BL, Muthu MS. Transferrin receptor-targeted vitamin E TPGS micelles for brain cancer therapy: preparation, characterization and brain distribution in rats. Drug Deliv. 2015;23(5):1788-98. doi:10.3109/10717544.2015.1094681.

9. Lee H, Fisher S, Kallos MS, Hunter CJ. Optimizing gelling parameters of gellan gum for fibrocartilage tissue engineering. J. Biomed. Mater. Res. Part B Appl. Biomater. 2011;98(2):238-45. doi:10.1002/jbm.b.31845.

10. Ahn JS, Kim KM, Ko CY, Kang JS. Absorption enhancer and polymer (Vitamin E TPGS and PVP K29) by solid dispersion improve dissolution and bioavailability of eprosartan mesylate. Bull. Korean Chem. Soc. 2011;32(5):1587-92. doi:10.5012/bkcs.2011.32.5.1587

11. Shin SC, Kim J. Physicochemical characterization of solid dispersion of furosemide with TPGS. Int. J. Pharm. 2003;251(1):79-84. doi:10.1016/s0378-5173(02)00586-0.

12. Vuddanda PR, Rajamanickam VM, Yaspal M, Singh S. Investigations on Agglomeration and Haemocompatibility of Vitamin E TPGS Surface Modified Berberine Chloride Nanoparticles. Biomed Res. 2014 Int. Article ID 951942. Doi:10.1155/2014/951942

13. Srivalli KMR, Mishra B. Improved Aqueous Solubility and Antihypercholesterolemic Activity of Ezetimibe on Formulating with Hydroxypropyl-β-Cyclodextrin and Hydrophilic Auxiliary Substances. AAPS PharmSciTech 2015;17(2):272-83. doi:10.1208/s12249-015-0344-7.

14. Zembko I, Ahmed I, Farooq A, Dail J, Tawari P, Wang W, Mcconville C. Development of Disulfiram-Loaded Poly(Lactic-co-Glycolic Acid) Wafers for the Localised Treatment of Glioblastoma Multiforme: A Comparison of Manufacturing Techniques. J. Pharm Sci. 2015;104:1076-86. doi:10.1002/jps.24304.

15. Yang F, Xia S, Tan C, Zhang X. Preparation and evaluation of chitosan-calcium gellan gum beads for controlled release of protein. Eur. Food Res. Technol. 2013;237:467-79. Doi:10.1007/s00217-013-2021-y.

16. Albertinia B, Passerinia N, Di Sabatinoa M, Monti D, Burgalassi S, Chetoni P, Rodriguez L. Poloxamer 407 microspheres for orotransmucosal drug delivery. Part I: Formulation, manufacturing and characterization. Int. J. Pharm. 2010;399:71–9. doi:10.1016/j.ijpharm.2010.08.004.